Synthetic nanopores with fixed charges: An electrodiffusion model for ionic transport

P. Ramírez*
Departament de Física Aplicada, Universitat Politècnica de València, Camino de Vera s/n, E-46022 Valencia, Spain

S. Mafé†
Departament de Termodinàmica, Facultat de Física, Universitat de València, E-46100 Burjassot, Spain

V. M. Aguilella‡ and A. Alcaraz§
Departament de Ciències Experimentals, Universitat Jaume I, Ap. 224, E-12080 Castelló, Spain

(Received 26 February 2003; published 25 July 2003)

Synthetic nanopores with fixed charges exhibit ionic equilibrium and transport properties that resemble those displayed by biological ion channels. We present an electrodiffusion model based on the Nernst-Planck flux equations, which allows for a qualitative description of the steady state ionic transport through a nanopore when the membrane fixed charges and all mobile carriers (including the water ions) are properly taken into account. In particular, we study the current-voltage curve, the electrical conductance, the reversal potential (a measure of the nanopore ionic selectivity), as well as the flux inhibition by protons and divalent cations in the nanopore. The model clearly shows how the changes in the ionization state of the fixed charges with *p*H and salt concentration dictate the electrical properties of the nanopore. The agreement between the model predictions and previous experimental data allows us to identify which are the main characteristics that permit a simple description of this complex system.

DOI: 10.1103/PhysRevE.68.011910 PACS number(s): 82.39.Wj, 87.16.Uv, 81.07.De

I. INTRODUCTION

The development of novel experimental techniques allows us to obtain synthetic nanopores displaying some of the characteristic properties of biological ion channels. One of these techniques is based on the irradiation of polymer films (or foils) with energetic heavy ions and subsequent chemical etching [1–7]. The analogy between synthetic nanopores and biochannels may be not only structural but also functional: narrow pores with fixed charges show some of the typical features of ion channels such as ionic selectivity, flux inhibition by protons and divalent cations, and ion current fluctuations between high and low conductance states [1,8]. These similarities reveal that the study of ion transport through synthetic nanopores can contribute not only to the development of new ionic sensors and electroresponsive devices, but also to a better understanding of biochannels [3,7,9]. Note also that although some of the characteristics of ion channels can be manipulated *in vitro* (e.g., by site-directed mutagenesis aimed at the modification of the functional groups [8,10]), the production of track-etched nanopores permits a better control of the density of fixed charges as well as the size and geometry of the pore. Therefore, synthetic nanopores may constitute appropriate tests for validating electrostatic and electrodiffusion models.

Most previous studies showing the analogies between synthetic nanopores and biochannels have focused on the techniques to produce the nanopores and the qualitative description of the experimental features observed. In this paper, we will show that mean field electrodiffusion models based on continuous diffusion-migration flux equations can offer simple and intuitive explanations to many of the observed phenomena when the membrane fixed charges and mobile ions are properly taken into account in the model, a question previously emphasized by Eisenberg (see, e.g., Ref. [11] and references therein) in the case of ionic channels. In particular, we will focus on the equilibrium and steady state properties of the nanopores (ionic selectivity, electrical properties, and flux inhibition by protons and divalent cations), leaving the ion current fluctuations between high and low conductance states for future studies addressing the time response of the system. Special attention will be paid to the functional groups (fixed charges) attached to the polymer backbone, since the changes in the ionization state of these charges with the *p*H and salt concentration of the external solution dictate the ionic transport properties of the nanopore.

The use of continuum models to describe ion transport in narrow pores is currently a matter of controversy. Although recent studies have questioned the validity of continuum, mean field theories in systems whose dimensions are comparable to the electrolyte Debye length [12,13], these theories appear to provide interesting clues to ion permeation even in ion channels a few nanometers thick having narrow regions less than 1 nm in radius [11,14–16]. (Apparently, mean field theories work better than expected in many cases [16,17].) We will focus our analysis on the experimental results obtained previously with poly(ethylene terephthalate) (PETP) membranes [1–3]. These filters were first subject to irradiation with energetic heavy ions to produce nuclear tracks, and subsequently etched with hot alkali to convert the tracks to pores by hydrolysis of the ester bonds, giving rise to weak

*Corresponding author. Electronic address: patraho@fis.upv.es
†Electronic address: smafe@uv.es
‡Electronic address: aguilell@uji.es
§Electronic address: alcaraza@uji.es

acid carboxylic groups in the pore surface [2]. The experimental results reported for two nanopores of length 5 μm and radii 1.0 and 1.4 nm [1] will be considered here. Because of the local electroneutrality condition, the total mobile ion concentration at every position in the pore is approximately that of the total fixed charge concentration when all the fixed charge groups are ionized. For the surface density of functional groups reported (1.6 functional groups/nm^2) [4], the fixed charge concentration for the nanopore with 1 nm radius is $\approx$5M (see Sec. III). This relatively high fixed charge concentration yields a typical Debye length in the membrane several times lower than the pore radius, a result that gives support to the use of a continuum treatment. Note also that the nanopore radii are close to those found in relatively large ion channels (e.g., the alamethicin channel [18] and the voltage-dependent anion channel in the mitochondrial outer membrane [19,20]) where continuum approaches are currently being used to model ionic selectivity and conductance data. Finally, since the nanopore length is relatively high, one would expect electrodiffusion through the pore rather than the concerted motion of a few ions or some specific interfacial process to be rate limiting. Therefore, thermodynamic quasiequilibrium at the membrane-solution interfaces is assumed, and the Donnan equations for all the ionic species present (the two salt ions and the proton and hydroxyl ions) will be considered.

If the fixed charges are weak acid groups [2,3], the ionic selectivity will depend on the local pH inside the pore, and this value can be significantly different from that in the external solutions because of the electrical coupling between all ionic species (see, e.g., Ref. [21] and references therein). Also, for the transport of the ionic species through the nanopore, the one-dimensional Nernst-Planck flux equations are used, taking into account both diffusion and migration. To this end, the resulting system of differential transport equations is solved using the Goldman assumption, which assumes that the electric field is constant over the spatial region where electrodiffusion occurs. For the conditions of high fixed charge concentration, small pH and concentration gradients, and negligible convection flow considered here, this assumption provides analytical expressions for the ion fluxes that constitute good approximations to those obtained by the numerical solution of the exact transport equations [22].

II. THEORY

The system considered is shown schematically in Fig. 1. The nanoporous PETP filter extends from $x=0$ to $x=d$ and consists of a porous polymeric backbone with pores of an average radius r. The filter separates two electrolyte aqueous solutions containing a mixture of KCl and $CaCl_2$, and we assume that the pH of the external solutions is controlled by adding either HCl or KOH. Therefore, in the most general case, the ionic mobile species present in the system are the salt ions (K^+, Ca^{2+}, Cl^-), and the hydrogen (H^+) and hydroxide (OH^-) ions. In Fig. 1, $c_{S,j}$ and $c_{S',j}$ are the KCl and $CaCl_2$ concentrations in solution j ($j=L$ for the left solution and $j=R$ for the right solution), respectively. The solutions

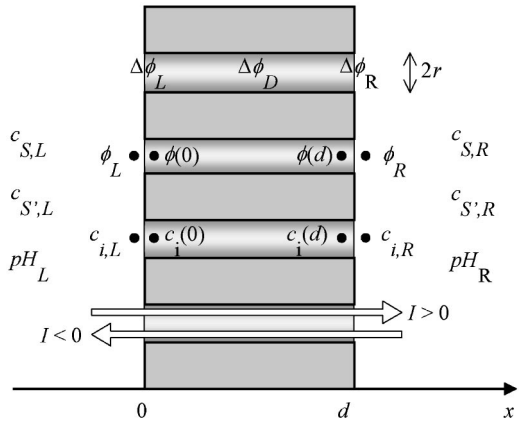

FIG. 1. Sketch of the system considered. The PETP filter extends from $x=0$ to $x=d$ and has monodisperse nanopores of radius r. The bathing solutions contain a mixture of KCl and $CaCl_2$ salts at concentrations c_{Sj} and $c_{S'j}$, respectively ($j=L,R$). c_{ij} is the concentration of the species i in the bulk of the external solution j. ϕ_j and $p\mathrm{H}_j$ refer to the electric potential and the pH value of the solution j, and $c_i(x)$ and $\phi(x)$ are the local concentration of the species i and the electric potential within the pore. $\Delta\phi_L=\phi(0)-\phi_L$ and $\Delta\phi_R=\phi_R-\phi(d)$ are the Donnan potential drops through the left and right interfaces, respectively, and $\Delta\phi_D=\phi(d)-\phi(0)$ the diffusion potential within the pore. Finally, I is the total electric current passing through the membrane under an applied potential difference $V=\phi_L-\phi_R$.

are assumed to be perfectly stirred, and the whole system is isothermal. Also, $c_{i,j}$ is the concentration of the species i ($i=K^+$, Ca^{2+}, H^+, Cl^-, and OH^-) in the bulk of the external solution j. ϕ_j and $p\mathrm{H}_j$ refer, respectively, to the electric potential and the pH value of the solution j. $c_i(x)$ and $\phi(x)$ are the local concentration of the species i and the local electric potential within the pore. $\Delta\phi_L=\phi(0)-\phi_L$ and $\Delta\phi_R=\phi_R-\phi(d)$ denote, respectively, the Donnan potential drops through the left and right interfaces, and $\Delta\phi_D=\phi(d)-\phi(0)$ is the diffusion potential within the pore. I is the total electric current passing through the membrane under an applied potential difference V. Finally, $X_F(x)$ is the total membrane fixed charge concentration at a point of coordinate x.

As mentioned in the Introduction, the nanopores contain weak acid carboxylic groups attached to the pore walls. We assume that these groups are homogeneously distributed on the pore surface. The neutral (-COOH) and dissociated ($-COO^-$) forms of the carboxylic groups are in equilibrium with the H^+ ions of the membrane solution,

$$-\mathrm{COOH} \overset{K_N}{\rightleftarrows} -\mathrm{COO}^- + \mathrm{H}^+, \tag{1}$$

where K_N is the equilibrium constant for the dissociation reaction. Also, Ca^{2+} may bind to $-COO^-$ according to the scheme

$$-\mathrm{COO}^- + \mathrm{Ca}^{2+} \overset{K_B}{\rightleftarrows} -\mathrm{COO}\cdots\mathrm{Ca}^+, \tag{2}$$

where K_B is the equilibrium constant for the binding reaction. The resulting $-COO\cdots Ca^+$ complex acts then as an

anion exchange group. Calcium binding to fixed charge groups is relevant in membranes [23], ion exchange fibers [24], phospholipid monolayers [25], and biomacromolecules [26].

From Eqs. (1) and (2), we obtain

$$10^{-pK_a} \equiv K_N = \frac{X_C^N c_{H^+}}{X_C^0}, \tag{3}$$

$$K_B = \frac{X_C^P}{X_C^N c_{Ca^{2+}}}, \tag{4}$$

where X_C^N, X_C^0, and X_C^P are the concentrations of negative (-COO^-), neutral (-COOH), and positive (-$COO\cdots Ca^+$) forms of the carboxylic groups, respectively. From Eqs. (3) and (4), together with

$$X_{CT} = X_C^P + X_C^N + X_C^0, \tag{5}$$

where X_{CT} is the total concentration of carboxylic groups, the effective membrane fixed charge concentration yields

$$X_F = X_C^P - X_C^N = \frac{K_B c_{Ca^{2+}} - 1}{1 + c_{H^+}/K_N + K_B c_{Ca^{2+}}} X_{CT}. \tag{6}$$

Note that for $pH \gg pK_a$, the effective membrane fixed charge concentration is $-X_{CT}$ when $K_B c_{Ca^{2+}} \ll 1$ (no calcium binding) and X_{CT} when $K_B c_{Ca^{2+}} \gg 1$.

For a given pH, the concentrations of H^+, OH^-, and Ca^{2+} in the external solutions are

$$c_{H^+,j} = 10^{-pH}, \quad j = L,R, \tag{7}$$

$$c_{OH^-,j} = K_W / c_{H^+}, \quad j = L,R, \tag{8}$$

$$c_{Ca^{2+},j} = c_{S',j}, \quad j = L,R, \tag{9}$$

where $K_W = 10^{-14} M^2$. Finally, the electroneutrality condition in the external solutions leads to

$$c_{K^+,j} + 2c_{Ca^{2+},j} + c_{H^+,j} = c_{Cl^-,j} + c_{OH^-,j}, \quad j = L,R. \tag{10}$$

For $pH \leqslant 7$, HCl is added, and then Eqs. (9) and (10) give

$$c_{K^+,j} = c_{S,j}, \quad j = L,R, \tag{11}$$

$$c_{Cl^-,j} = c_{S,j} + 2c_{S',j} + c_{H^+,j} - c_{OH^-,j}, \quad j = L,R. \tag{12}$$

For obtaining $pH > 7$, KOH is added, and Eqs. (9) and (10) give

$$c_{Cl^-,j} = c_{S,j} + 2c_{S',j}, \quad j = L,R, \tag{13}$$

$$c_{K^+,j} = c_{S,j} - c_{H^+,j} + c_{OH^-,j}, \quad j = L,R. \tag{14}$$

The external and pore solution concentrations are connected through the following Donnan equilibrium conditions [27]:

$$c_i(0) = c_{i,L} \exp\left(-\frac{z_i F}{RT} \Delta\phi_L \right), \tag{15}$$

$$c_i(d) = c_{i,R} \exp\left(\frac{z_i F}{RT} \Delta\phi_R \right), \tag{16}$$

at the interfaces $x = 0$ and $x = d$ (see Fig. 1), where z_i is the charge number of species i and the partition coefficients have been assumed to be unity [27]. To assume interfacial equilibrium is a reasonable approximation here: since the pore length ($\sim 5 \times 10^{-6}$ m) is much higher than the pore radius ($\sim 10^{-9}$ m) [1–4], electrodiffusion through the pore rather than interfacial resistance should be rate limiting for ionic transport [27]. (Note, however, that by considering such long synthetic nanopores, we are implicitly ignoring one of the salient features of the selectivity filters in ion channels: the concerted motion of a few ions over regions of the order of 1 nm thick [8].)

Combining Eqs. (15) and (16) with the electroneutrality condition inside the pore,

$$\sum_i z_i c_i + X_F = 0, \tag{17}$$

we find the following equations:

$$\left(1 + \frac{c_{K^+,j}}{c_{H^+,j}} \right) u_j + 2 \frac{c_{Ca^{2+},j}}{c_{H^+,j}} u_j^2 + \frac{X_F}{c_{H^+,j}} - \frac{c_{Cl^-,j} + c_{OH^-,j}}{c_{H^+,j}} \frac{1}{u_j} = 0, \quad j = L,R, \tag{18}$$

where $u_L \equiv c_{H^+}(0)/c_{H^+,L}$ and $u_R \equiv c_{H^+}(d)/c_{H^+,R}$. Equation (18) can be readily solved for u_j using a numerical procedure. After determining u_j, the pore concentrations $c_i(0)$ and $c_i(d)$ can be obtained from Eqs. (15) and (16) in terms of the concentrations of the different species in the adjacent external solutions. Once all the concentrations $c_i(0)$ and $c_i(d)$ are known, the Donnan potential differences through the left and right interfaces, $\Delta\phi_L$ and $\Delta\phi_R$, can be also computed.

We assume that the flux J_i of species i through the nanopores is described by the Nernst-Planck equations

$$J_i = -D_i \frac{dc_i}{dx} - z_i D_i c_i \frac{F}{RT} \frac{d\phi}{dx}, \tag{19}$$

where D_i is the diffusion coefficient of species i in the pore solution, and constants F, R, and T have their usual meaning [27]. The total electric current passing through a single pore is given by

$$I = F \pi r^2 \sum_i z_i J_i, \tag{20}$$

and the potential difference (voltage) applied to the system can be written as

$$V = -(\Delta\phi_L + \Delta\phi_D + \Delta\phi_R). \tag{21}$$

Equations (3)–(6), (17), and (19)–(21) constitute a set of algebraic and differential equations. This boundary value problem could be solved using an iterative scheme [28] but in order to obtain analytical solutions for the ionic fluxes

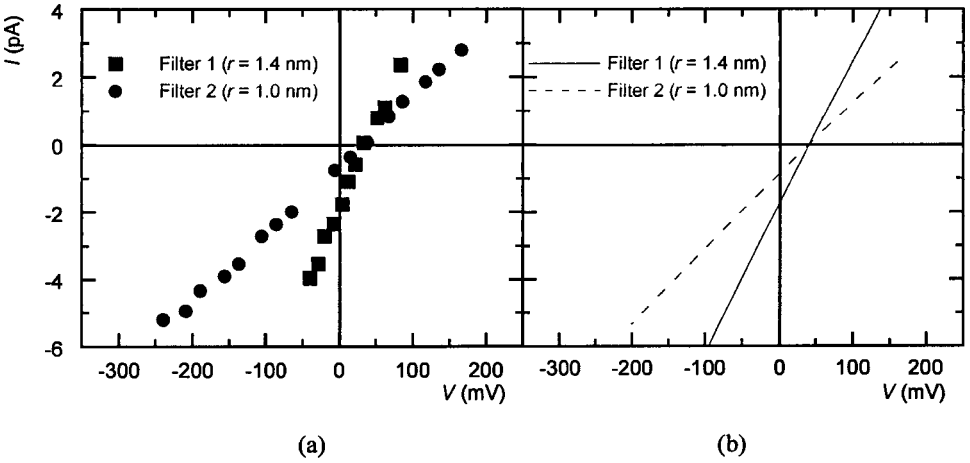

FIG. 2. Current-voltage curves of single nanopores in two PETP filters. Experimental data in (a) are taken from Ref. [1]. The concentrations of KCl in the bathing solutions were $c_{S,L}=0.1M$ and $c_{S,R}=0.5M$ with $p\mathrm{H}_L=p\mathrm{H}_R=7.4$. The solid and dashed lines in (b) correspond to the theoretical results using $D_{\mathrm{K}^+}=1.95\times10^{-5}$ cm^2/s, $D_{\mathrm{Cl}^-}=2.03\times10^{-5}$ cm^2/s, $D_{\mathrm{H}^+}=9.0\times10^{-5}$ cm^2/s, and $D_{\mathrm{OH}^-}=4.5\times10^{-5}$ cm^2/s, with $X_{CT}=5M$ and $p\mathrm{K}_a=5$.

(assumed to be approximately constant) we use the Goldman constant field (GCF) approximation which considers a constant electric field through the membrane [22,29]. Although these approximations are crude, the results obtained give the qualitative theoretical trends of the model, especially, when the membrane fixed charge concentration is high and the pH and concentration gradients through the membrane are small [22,30,31]. Previous studies on different membrane systems have shown that the GCF approximation gives estimates for the ionic fluxes that can be compared to those obtained by the numerical solution of the exact transport equations [29–31]. Note finally that this approximation allows us to linearize the Nernst-Planck equations [see Eq. (19)] and this leads to a simple analytic solution. Indeed, the fluxes of the different ionic species can then be written in the form

$$J_i \approx \frac{z_i F}{RT}\frac{D_i \Delta\phi_D}{d}\frac{c_i(0)\exp(-z_i F\Delta\phi_D/RT)-c_i(d)}{1-\exp(-z_i F\Delta\phi_D/RT)}. \tag{22}$$

The current-voltage (I-V) curve can now be obtained as follows. Given an applied voltage V, the diffusion potential $\Delta\phi_D$ is calculated from Eq. (21). Substituting for $\Delta\phi_D$ in Eq. (22), the fluxes of all the ionic species are determined, and the total electric current is finally calculated using Eq. (20).

Once the total electric current has been calculated, the conductance of the membrane is given by

$$G=I/V. \tag{23}$$

Finally, substituting Eqs. (22) in Eq. (20) for $I=0$, we obtain

$$\sum_i \frac{z_i^2 F}{RT}\frac{D_i \Delta\phi_D}{d}\frac{c_i(0)\exp(-z_i F\Delta\phi_D/RT)-c_i(d)}{1-\exp(-z_i F\Delta\phi_D/RT)}=0. \tag{24}$$

Equation (24) can be solved for $\Delta\phi_D$ using a numerical procedure. Finally, the ion fluxes and the potential difference under open circuit conditions ($I=0$), i.e., the so called reversal potential

$$V_{\mathrm{rev}}=-(\Delta\phi_L+\Delta\phi_D+\Delta\phi_R), \tag{25}$$

can also be computed.

III. RESULTS AND DISCUSSION

We have compared the results provided by the above theoretical model with the experimental data by Pasternak and co-workers [1] on the electrical properties of PETP nanoporous membranes. These data cover a wide variety of experimental situations concerning I-V curves, membrane conductance, reversal potential, and inhibition of conductance by H^+ and Ca^{2+} ions adsorbed onto the pore walls. Both pH and salt concentration effects are studied.

The experimental data in Fig. 2(a) correspond to the I-V curves obtained from two PETP filters with nanopores of radii $r=1.4$ nm (filter 1) and $r=1.0$ nm (filter 2) in the presence of a KCl concentration gradient ($c_{S,L}=0.1M$ and $c_{S,R}=0.5M$) at $p\mathrm{H}_L=p\mathrm{H}_R=7.4$. No CaCl_2 was added to the bathing solutions ($c_{S',L}=c_{S',R}=0$). The thickness of both filters was $d=5$ μm, and contained ≈1 pore per cm^2. We see that the I-V curves show a linear behavior over the whole range of voltages applied. The intercept of the curves with the horizontal axis ($I=0$) corresponds to the reversal potential $V_{\mathrm{rev}}\approx35$ mV regardless of the pore radius. The slope of each curve gives the conductance of the nanopore. The measured values are $G=51$ pS for $r=1.4$ nm and $G=20$ pS for $r=1.0$ nm. The lines in Fig. 2(b) correspond to the theoretical results obtained with the infinite dilution diffusion coefficients $D_{\mathrm{K}^+}=1.95\times10^{-5}$ cm^2/s, $D_{\mathrm{Cl}^-}=2.03\times10^{-5}$ cm^2/s, $D_{\mathrm{H}^+}=9.0\times10^{-5}$ cm^2/s, and $D_{\mathrm{OH}^-}=4.5\times10^{-5}$ cm^2/s. The concentration of weak carboxylic groups in the filter was estimated as follows. The surface density of ionizable groups, σ, is related to the volumic concentration of carboxylic groups, X_{CT} through the electroneutrality condition

$$\sigma 2\pi r de = F X_{CT}\pi r^2 d, \tag{26}$$

where $e=1.6\times10^{-19}$ C is the elementary charge. Bashford, Alder, and Pasternak [4] have reported the value $\sigma\approx1.6$ groups/nm^2 in PETP membranes, and Eq. (26) gives $X_{CT}\approx5M$ for $r\approx1$ nm. Therefore, the only unknown parameter in the calculations is the $p\mathrm{K}_a$ value of the carboxylic groups. In free solution, this $p\mathrm{K}_a$ is in the range 3–5, but

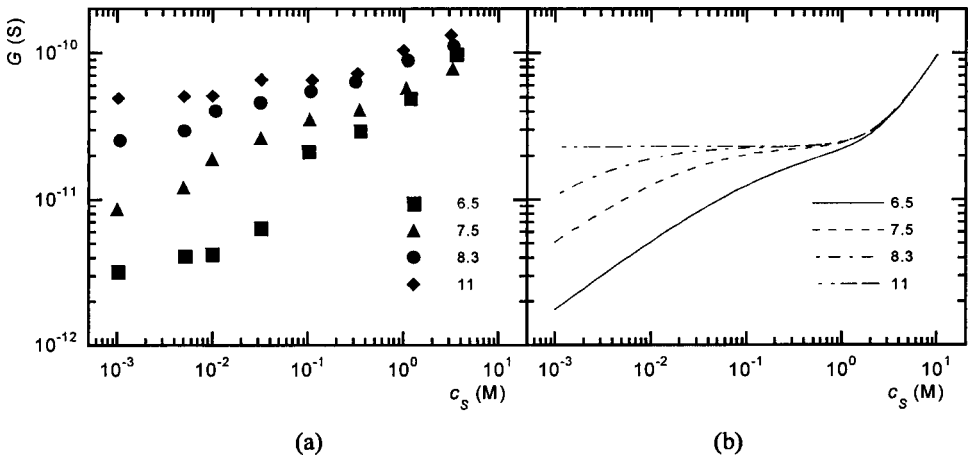

FIG. 3. Conductance of a PETP filter containing a single nanopore ($r=1.0$ nm, filter 2). The experimental data [1] in (a) are parametric in $p\mathrm{H}\equiv p\mathrm{H}_L=p\mathrm{H}_R$ (see symbols). The applied voltage was $V=0.8$ V. The filter separated two identical KCl solutions of concentrations $c_{S,L}=c_{S,R}\equiv c_S$. The theoretical results in (b) are obtained using the same values for the model parameters as in Fig. 2(b).

apparent $p\mathrm{K}_a$ values in the range 6–10 have also been reported in self-assembled monolayers formed from thiols on flat gold surfaces and long-chain fatty acids [32–34]. We have tentatively used $p\mathrm{K}_a=5$ in the calculations of Fig. 2(b) (see also Figs. 3–6 later). Bearing in mind the crude assumptions made, the theoretical results show a reasonable agreement with experimental data: the calculated value for the reversal potential is $V_{\mathrm{rev}}\approx 40$ mV, and the conductances predicted are $G=44$ pS for $r=1.4$ nm and $G=22$ pS for $r=1.0$ nm, which corresponds to deviations of ca. 10% from the experimental values.

The experimental data in Fig. 3(a) illustrate the dependence of the conductance of filter 2 on the ionic strength of the bathing solutions. The filter separated two identical KCl solutions at the concentrations $c_S\equiv c_{S,L}=c_{S,R}$ indicated on the horizontal axis. No $CaCl_2$ was added to these solutions. The applied voltage was $V=0.8$ V, and the curves are parametric in the pH of the bathing solutions. We see that the pore conductances reported are in the range 3–100 pS and, for a fixed concentration of the bathing solutions, they increase with pH. We also see that the experimental points tend to group together as the concentration of the bathing solutions increases, reaching the value $G\approx 10^{-10}$ S for a concentrated KCl solution. The curves in Fig. 3(b) correspond to the theoretical results obtained using the same values for the model parameters as in Fig. 2(b). The theoretical curves agree qualitatively with the experimental behavior, although quantitative discrepancies can be found, especially at high pH values. For instance, at $p\mathrm{H}=11$ and $c_S=10^{-3}M$, the experimental conductance is $G\approx 500$ pS, while the model gives only 230 pS. These discrepancies should be ascribed to effects not included in the theoretical model: the pH of the bathing solutions might affect the effective radius of the nanopores and the concentration of the solution inside the pore could change the effective $p\mathrm{K}_a$ value of the carboxylic groups. Moreover, 0.1–3 mM ethylenediamine tetra-acetic acid (EDTA) and 5-mM HEPES were used as buffers in the experiments to fix the pH value of the bathing solutions. It is not clear how these compounds, not considered in the model, may affect the conductance of the nanopore, especially for low c_S values, where the concentrations of the buffers are comparable to that of the electrolyte. In any case, the model is able to explain the basic features of the conductance curves: G increases with the pH approximately by one order of magnitude at low electrolyte concentrations and attains a limit value at high electrolyte concentrations.

Figure 4(a) shows the experimental results for the reversal potential V_{rev} of a nanoporous PETP filter separating two KCl solutions of different concentrations vs $p\mathrm{H}\equiv p\mathrm{H}_L=p\mathrm{H}_R$. In these measurements (unpublished results), a PETP filter with 10^9 pores/cm^2 was used. Again, 0.1-mM EDTA and 5-mM HEPES were employed as buffers in order to keep the pH constant. The experimental points correspond

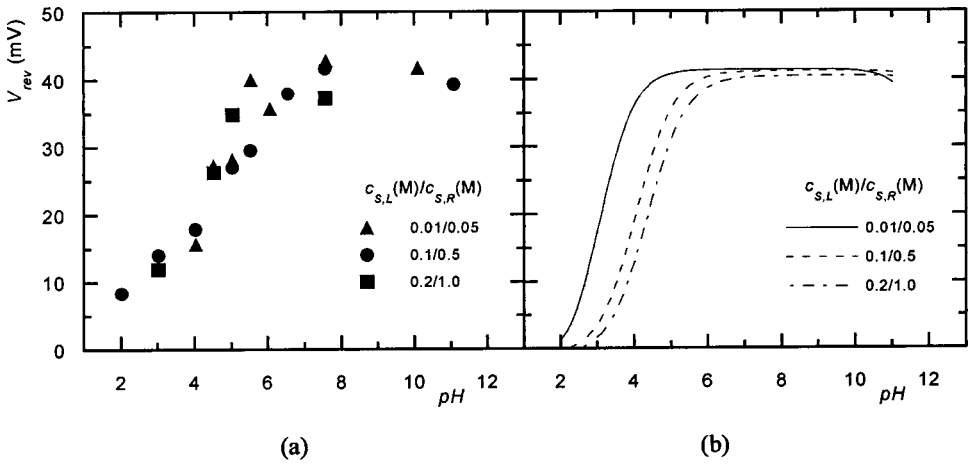

FIG. 4. Reversal potential V_{rev} of a nanoporous PETP filter vs $p\mathrm{H}\equiv p\mathrm{H}_L=p\mathrm{H}_R$. The experimental data [35] in (a) correspond to a PETP filter with 10^9 pores/cm^2 separating two KCl solutions at the concentration ratios $c_{S,R}/c_{S,L}$ of the figure (see symbols). The theoretical curves in (b) are obtained using the same values for the model parameters as in Figs. 2(b) and 3(b).

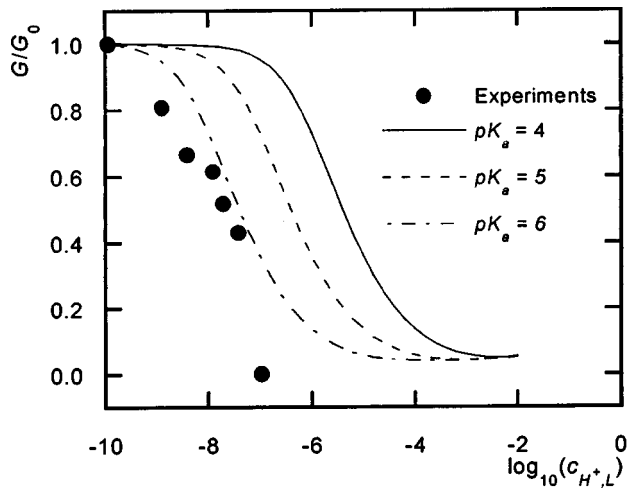

FIG. 5. Effect of H^+ concentration on the inhibition of the pore conductance of a PETP filter. Experimental data (circles) [1] correspond to a single nanopore ($r \approx 1.4$ nm, filter 1) separating two $0.1M$ KCl solutions. The conductance (G) relative to the maximum observed conductance (G_0) is plotted vs $\log_{10}(c_{H^+,L})$ with $c_{H^+,L} = c_{H^+,R}$ for an applied voltage $V = 0.2$ V. The theoretical curves are parametric in the pK_a value of carboxylic groups, and the model parameters are the same as in Figs. 2(b), 3(b), and 4(b).

to different KCl concentration ratios $c_{S,R}/c_{S,L}$, and no $CaCl_2$ was added to the surrounding solutions ($c_{S',L} = c_{S',R} = 0$). The theoretical results in Fig. 4(b) are calculated with the same values for the model parameters as in Figs. 2(b) and 3(b). Again, the theoretical curves agree qualitatively with the experimental data. For pH values in the range 6–11, all carboxylic groups in the filter pores are deprotonated, and the concentrations of K^+ and Cl^- are much higher than those of H^+ and OH^-. Therefore, the reversal potential attains the constant Nernstian value $V_{rev} \approx (RT/F)\ln(c_{S,R}/c_{S,L}) \approx 41$ mV characteristic of an ideally selective membrane (note that the concentration of fixed charges $X_{CT} = 5M \gg c_{S,L}$, $c_{S,R}$). At low enough pH values, however, all the carboxylic groups in the filter pores are protonated, and the concentration of fixed charges is approximately zero. Therefore, the Donnan potential drops at the membrane-solution interfaces vanish, and the reversal potential is approximately equal to the diffusion potential. Since we have assumed the infinite dilution values $D_{K^+} = 1.95 \times 10^{-5}$ cm^2/s $\approx D_{Cl^-} = 2.03 \times 10^{-5}$ cm^2/s for the diffusion coefficients, the diffusion potential (and therefore the reversal potential) attains very small values. (Note again that under such conditions, the contribution of the buffer to the measured potential could still be noticeable.) The transition between the two regions above occurs in the range $3 < p\mathrm{H} < 6$. The position and the slope of the curves in this range is determined by the pK_a value of the carboxylic groups. Again, a reasonable agreement between theory and experiments is found for $pK_a = 5$, as in Fig. 2.

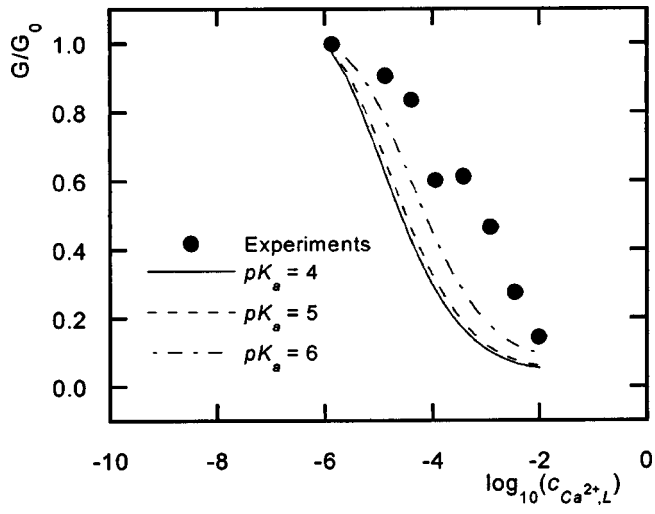

FIG. 6. Effect of Ca^{2+} addition on the inhibition of the pore conductance of a PETP filter. Experimental data (circles) [1] correspond to the same PETP filter as in Fig. 5 separating two $0.1M$ KCl solutions at $p\mathrm{H} \equiv p\mathrm{H}_L = p\mathrm{H}_R = 7.4$. G/G_0 is plotted vs $\log_{10}(c_{Ca^{2+},L})$ with $c_{Ca^{2+},L} = c_{Ca^{2+},R}$. The applied voltage is $V = 0.2$ V. The theoretical curves are parametric in the pK_a value of carboxylic groups, and the model parameters are the same as in Figs. 2(b), 3(b), 4(b), and 5.

The inhibition effect of H^+ and Ca^{2+} ions on the pore conductance is shown in Figs. 5 and 6. As mentioned in the Introduction, this inhibition may constitute one of the functional analogies between synthetic nanopores and biochannels. The experimental points correspond to a PETP filter with a single nanopore of radius $r \approx 1.4$ nm (filter 1) separating two $0.1M$ KCl solutions. The conductance (G) under an applied voltage $V = 0.2$ V was scaled to the maximum observed conductance (G_0). In the experiments, HCl or KOH (Fig. 5) and $CaCl_2$ (Fig. 6) were added to the KCl solutions in order to change the H^+ (Fig. 5) and the Ca^{2+} (Fig. 6) concentrations. The initial pH of the solutions was 7.4 in both experiments. The theoretical calculations (solid and dashed curves) are parametric in the pK_a value of carboxylic groups. For the curves of Fig. 6, we have employed $K_B = 10^2 M^{-1}$ as a typical value for the binding constant of Ca^{2+} to the carboxylic groups (K_B appears to be in the range $(10-10^3)M^{-1}$ for ion exchange filters and phospholipid membranes [24,25] though significantly higher binding constants up to $10^5 M^{-1}$ have been reported for trivalent (La^{3+}) cations [25]). The values used in the calculations for the other parameters in the theoretical model are the same as in Figs. 2–4.

The experimental data in Fig. 5 show that the pore conductance of PETP membranes decreases when the concentration of H^+ in the bathing solutions increases (i.e., when the pH decreases). This reflects the titration curve of carboxylic groups: at low concentration of H^+ (high pH values), all the carboxylic groups in the nanopore are in charged form, and the conductance of the nanopore is high. As the concentration of H^+ increases, more and more carboxylic groups protonate. Therefore, the concentration of fixed charges decreases and so does the nanopore conductance which is proportional to the mobile ions compensating for the fixed charges. We see that the theoretical results obtained with this relatively simple model reproduce qualitatively the experimental trends. Again, a reasonable agreement between theory

and experiments is achieved when the pK_a of the carboxylic groups is assumed to be in the range 5–6.

The experimental points in Fig. 6 show a similar behavior for the relative pore conductance when Ca^{2+} is added to the bathing solutions. We can ascribe the inhibition of the nanopore conductance to the adsorption of Ca^{2+} to the carboxylic groups, giving rise to a sort of ''electrostatic blocking'' [8] (see also Ref. [36]). The presence of adsorbed Ca^{2+} reduces the effective concentration of fixed charge in this cation selective nanopore, decreasing the conductance accordingly. Assuming a typical value for the binding constant, the model describes the experimental trends qualitatively. Again, a good agreement between theory and experiments is achieved when the pK_a value of the carboxylic groups is close to 6, although the calculations are not as sensitive to the pK_a value as those in Fig. 5.

In summary, we have presented a simple model accounting for the ionic transport through PETP filters containing approximately cylindrical pores of an average radius of the order of 1 nm. In spite of the crude assumptions made, the theoretical results provide qualitative explanations for the current-voltage curve, the conductance vs electrolyte concentration curves, the reversal potential, and the conductance inhibition by protons and divalent cations [1]. The agreement between the model predictions and previous experimental data clearly shows which are the main characteristics that allow a simple description of this complex system. In particular, the relatively high fixed charge concentration yields a typical Debye length in the membrane several times lower than the pore radius. Therefore, shielding effects are important, and this gives support to the use of a continuum treatment [37–39]. We expect the results to be of relevance for the understanding of ionic transport through synthetic fixed charge nanopores as well as for the simulation of some effects present in biomembranes.

ACKNOWLEDGMENTS

Financial support from the CICYT, Ministerio de Ciencia y Tecnología, Project No. MAT2002-00646 and the Fondo Europeo para el Desarrollo Regional (FEDER) is gratefully acknowledged. V.M.A. and A.A. thank Fundació Caixa-Castelló (Project No. P1-1B2001-20) and MCYT (Project No. BFM2000-329) for financial support.

[1] A. A. Lev, Y. E. Korchev, T. K. Rostovtseva, C. L. Bashford, D. T. Edmonds, and C. A. Pasternak, Proc. R. Soc. London, Ser. B **252**, 187 (1993).
[2] C. A. Pasternak, C. L. Bashford, Y. E. Korchev, T. K. Rostovtseva, and A. A. Lev, Colloids Surf., A **77**, 119 (1993).
[3] C. A. Pasternak, G. M. Alder, P. Y. Apel, C. L. Bashford, Y. E. Korchev, A. A. Lev, T. K. Rostovtseva, and N. I. Zhitariuk, Nucl. Instrum. Methods Phys. Res. B **105**, 332 (1995).
[4] C. L. Bashford, G. M. Alder, and C. A. Pasternak, Biophys. J. **82**, 2032 (2002).
[5] Z. Siwy, Y. Gu, H. A. Spohr, D. Baur, A. Wolf-Reber, R. Spohr, P. Apel, and Y. E. Korchev, Europhys. Lett. **60**, 349 (2002).
[6] Z. Siwy and A. Fulinski, Phys. Rev. Lett. **89**, 198103 (2002).
[7] Z. Siwy, D. Dobrev, R. Neumann, C. Trautmann, and K. Voss, Appl. Phys. A: Mater Sci. Process **76**, 781 (2003).
[8] B. Hille, *Ionic Channels of Excitable Membranes*, 2nd ed. (Sinauer Associates, Sunderland, MA, 1992).
[9] P. Apel, Y. E. Korchev, Z. Siwy, R. Spohr, and M. Yoshida, Nucl. Instrum. Methods Phys. Res. B **184**, 337 (2001).
[10] S. Peng, M. E. Blachly-Dyson, M. Forte, and M. Colombini, Biophys. J. **62**, 123 (1992).
[11] B. Eisenberg, Contemp. Phys. **171**, 1 (1999).
[12] B. Corry, S. Kuyucak, and S. H. Chung, Chem. Phys. Lett. **320**, 35 (2000).
[13] G. Moy, B. Corry, S. Kuyucak, and S. H. Chung, Biophys. J. **78**, 2349 (2000).
[14] M. G. Kurnikova, R. D. Coalson, P. Graf, and A. Nitzan, Biophys. J. **76**, 642 (1999).
[15] W. Nonner and B. Eisenberg, Biophys. J. **75**, 1287 (1998).
[16] W. Nonner, D. P. Chen, and B. Eisenberg, J. Gen. Physiol. **113**, 773 (1999).
[17] D. G. Levitt, J. Gen. Physiol. **113**, 789 (1999).
[18] V. M. Aguilella and S. M. Bezrukov, Eur. Biophys. J. **30**, 233 (2001).
[19] M. Zizi, M. C. Byrd, R. Boxus, and M. Colombini, Biophys. J. **75**, 704 (1998).
[20] V. Levadny, M. Colombini, X. X. Li, and V. M. Aguilella, Biophys. J. **82**, 1773 (2002).
[21] P. Ramírez, S. Mafé, and A. Tanioka, in *Encyclopedia of Surface and Colloid Science*, edited by A. Hubbard (Marcel Dekker, New York, 2002), p. 3927.
[22] J. Pellicer, S. Mafé, and V. M. Aguilella, Ber. Bunsenges. Phys. Chem. **90**, 867 (1986).
[23] T. S. Sørensen and S. R. Rivera, in *Surface Chemistry and Electrochemistry of Membranes*, edited by T. S. Sørensen, Surfactant Science Series Vol. 79 (Marcel Dekker, New York, 1999), p. 313.
[24] T. Jaskari, M. Vuorio, K. Kontturi, J. A. Manzanares, and J. Hirvonen, J. Controlled Release **70**, 219 (2001).
[25] S. A. Tatulian, in *Surface Chemistry and Electrochemistry of Membranes* (Ref. [23]), p. 871.
[26] T. L. Hill, *Cooperative Theory in Biochemistry* (Springer-Verlag, New York, 1985).
[27] N. Lakshminarayanaiah, *Equations of Membrane Biophysics* (Academic, New York, 1984).
[28] W. H. Press, B. P. Flannery, S. A. Teukolsky, and W. T. Vetterling, *Numerical Recipes* (Cambridge University Press, Cambridge, 1989).
[29] P. Ramírez, A. Alcaraz, S. Mafé, and J. Pellicer, J. Membr. Sci. **161**, 143 (1999).
[30] P. Ramírez, A. Alcaraz, and S. Mafé, J. Colloid Interface Sci. **242**, 164 (2001).
[31] P. Ramírez, A. Alcaraz, S. Mafé, and J. Pellicer, J. Membr. Sci. **135**, 135 (1997).
[32] Z. Hou, N. L. Abbott, and P. Stroeve, Langmuir **16**, 2401 (2000).
[33] H. H. Rmaile and J. B. Schlenoff, Langmuir **18**, 8263 (2002).

[34] J. R. Kanicky and D. O. Shah, J. Colloid Interface Sci. **256**, 201 (2002).
[35] T. K. Rostovtseva (private communication).
[36] W. Nonner, D. P. Chen, and B. Eisenberg, Biophys. J. **74**, 2327 (1998).
[37] D. Gillespie and R. S. Eisenberg, Biophys. J. **31**, 454 (2002).
[38] D. Gillespie and R. S. Eisenberg, Phys. Rev. E **63**, 061902 (2001).
[39] B. Eisenberg, Biophys. J. **100**, 507 (2003).